Optical-microphysical properties of pyrolysis smokes as judged from data of polarization spectronephelometry

R.F. Rakhimov, V.S. Kozlov, E.V. Makienko, and V.P. Shmargunov

Institute of Atmospheric Optics,
Siberian Branch of the Russian Academy of Sciences, Tomsk

Received December 29, 2001

Variations of smoke aerosol microstructure at the stages immediately following thermal decomposition of hydrocarbon compounds are analyzed based on laboratory measurements of light-scattering parameters with a polarization spectral nephelometer. Peculiarities of variations of the disperse composition and optical constants of aerosol particles at different modes of their formation are considered through direct modeling of aerosol scattering parameters and solution of the inverse problem. Estimates show that at different stages of wood smoke evolution, several maxima are observed in the size spectrum at particle radii of 0.08, 0.25, and 0.45 μm. The imaginary part of the refractive index of particles did not exceed 0.004, and the real part varied from 1.48 to 1.57. The increase of the pyrolysis temperature resulted in significant burning-out of the coarsest fraction and increase of the real and, especially, imaginary parts of the refractive index up to 0.05.

Introduction

Aerosols generated at thermal decomposition of hydrocarbon compounds undergo complex set of physical and chemical processes, which are poorly studied by now, and, in particular, processes determining the intensity of generation of absorbing components, for example, soot. Two methods are largely used to determine the microstructure of smoke aerosols. The first one is the contact method based on particle sampling onto specialized plates and taking electron-microscope photographs, and the second one is the optical method based on the use of the laws of light scattering and absorption in a dispersed medium. Application of the optical method to investigation of smoke aerosols is considered in Refs. 1–4, which present the estimated disperse structure and refractive index. In particular, the characteristic tendencies were separated in variation of the smoke size spectrum as the smoke was let to stay, and the refractive index was assessed.[1,2] In Refs. 5 and 6, variations of the microstructure were analyzed based on measurement of the polarization scattering phase functions with an angle-scanning nephelometer at the wavelength of 0.63 μm and direct simulation of aerosol scattering parameters with the use of the diagram approach. The results of numerical simulation of the kinetics of coagulation transformation of the disperse structure of a dense smoke[5] make clear the cause for appearance of a maximum ($r \sim 0.3$ μm) in the size spectrum.

Techniques for measurement and preliminary data processing

Measurement of spectral dependences of scattering characteristics of pyrolysis smokes are considered in this paper as a basis for more detailed study of microphysical properties of smoke aerosol. Analyzing angular spectral scattering functions, we can obtain information about polarization scattering phase functions in a wide wavelength range and thus increase the information capacity of the developed optical approach to solution of inverse problems.

A quite wide range of polarization spectral nephelometers for studying optical and microphysical aerosol properties under field and laboratory conditions[3,4,8,9] is now known. The use of a fixed number of scattering angles allowed relatively small-size setups to be made and provided for the possibility of performing real-time flow-through aerosol measurements. In this paper we analyze the data obtained with a spectral nephelometer from Ref. 5, which is capable of measuring polarization components of the scattering phase function in a 5-liter aerosol chamber in the wavelength range $\lambda = 0.4–0.7$ μm and at the scattering angle $\theta = 15, 45, 110, 135, 165°$.

Pyrolysis smokes were generated at thermal decomposition of wood (10 g, pine) in a heating cell with controlled temperature. The cell was installed in a specialized smoke chamber having the volume of 0.1 m^3. The chamber housed the heating (from 30 up to 1000°C) cell, a humidifier, and a UV radiation source. A closed airline was vented before every measurement cycle for a certain smoke (1.5 to 2 hours since the moment of smoke generation) with pure air through a set of AFA aerosol filters.

Tentative analysis of recorded optical signals just after termination of thermal decomposition of a wood sample in the heater has shown that for some time (about 5–7 minutes) the recorded light scattering parameters manifest random fluctuations caused by the inhomogeneous distribution of smoke particles in the analyzed flow as it enters the nephelometer cell.

0235-6880/02/004 292-08 $02.00

To decrease the influence of random fluctuations of optical signals before the beginning of spectral measurements, smokes were let to stay for a preset time. Then a fan blew smoke aerosols through hoses into the nephelometer cell, where scattering parameters were measured in the flow-through mode. Thus, for analysis we used measured data obtained at the stage of monotonic decrease of recorded signals for different conditions of smoke generation.

One cycle of spectral measurements took 7 to 10 minutes. Therefore, the initial data were synchronized to decrease the errors in spectral dependences of light scattering parameters due to aerosol variations and non-simultaneity of records at different wavelengths.

Toward this end, the monotonically decreasing time dependences of the directional scattering coefficients at every angle and every wavelength were approximated by exponential functions of time using the method of least squares. Then all values of the synchronized spectral curve were formed (from the obtained family of exponential dependences for five angles and nine wavelengths) based on the values calculated for the same time.

The estimates have shown that the mean error in approximation of the measured data did not exceed 3 to 7%.

Temporal variations of measured and scaled (reduced to the same scale) spectral dependences of the directional scattering coefficient at the angle $\theta = 45°$ are exemplified in Fig. 1.

Synchronization of the data actually enables us to decrease the measurement errors caused by quick dynamics of variations, which would be ~ 30–40% at the initial stage. Figure 1*b* illustrates the characteristic temporal dynamics of the spectral dependence of the directional scattering coefficient caused by the specificity of generation and subsequent transformation. A noteworthy fact is transformation of the spectral behavior of the parameter under study from the usual monotonically decreasing dependence at the initial stage of the processes to the "anomalous" one with a stable well pronounced maximum near $\lambda = 0.60$ μm.

The obtained experimental data were pre-analyzed through comparison with the results of direct numerical simulation of aerosol scattering parameters based on the Mie theory. The comparison was performed for both angular and spectral scattering functions. Besides, we analyzed the diagrams of joint variations of the parameters determining the shape of polarization scattering phase functions, in particular, the ratios $A_s = g(15°)/g(110°)$ and $D_s = g(165°)/g(110°)$, which characterize the forward and backward peaks of the scattering phase function, and the degrees of linear polarization at the angles $\theta = 110$ and 165° denoted as P_{110} and P_{165}, respectively.

Analysis of mutual variations of the shape parameters of the scattering phase function and the degree of polarization for different modes of smoke generation and development enables us to reveal peculiarities in the aerosol microstructure. In particular, the parameter characterizing the forward peak of the scattering phase function A_s varies within the characteristic range from 30 to 80, and the degrees of polarization P_{110} and P_{165} achieve rather high negative values of 0.2 and 0.6, respectively. This evidences that the smokes under study are disperse systems, and the particles with the radii of 0.2 to 0.4 μm dominate in their volume distribution. The observed values of the parameter characterizing the backward peak of the scattering phase function $D_s > 1$, in their turn, show that the considered pyrolysis wood smokes are weakly absorbing. At the same time, the scattering phase functions of the slightly sloping type ($D_s < 1$) are observed in the mode of combustion with flame, and this is a typical sign of manifestation of absorbing properties. The mentioned peculiarities of manifestation of the microphysical properties are in a good agreement with the data of Ref. 7.

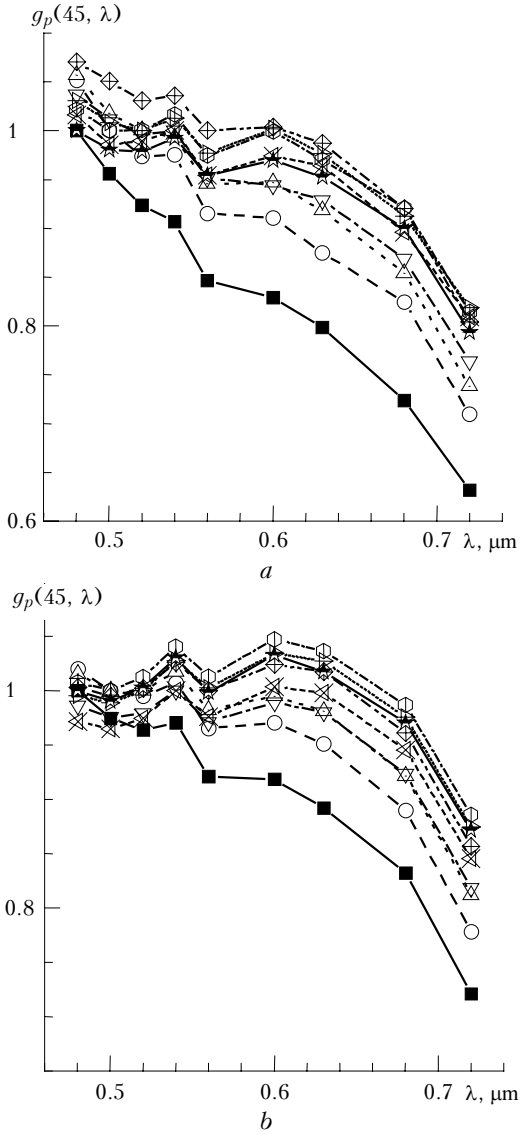

Fig. 1. Effect of synchronization on the spectral dependences of the scaled directional scattering coefficient at the angle of 45°: before synchronization (*a*) and after synchronization of measured data (*b*).

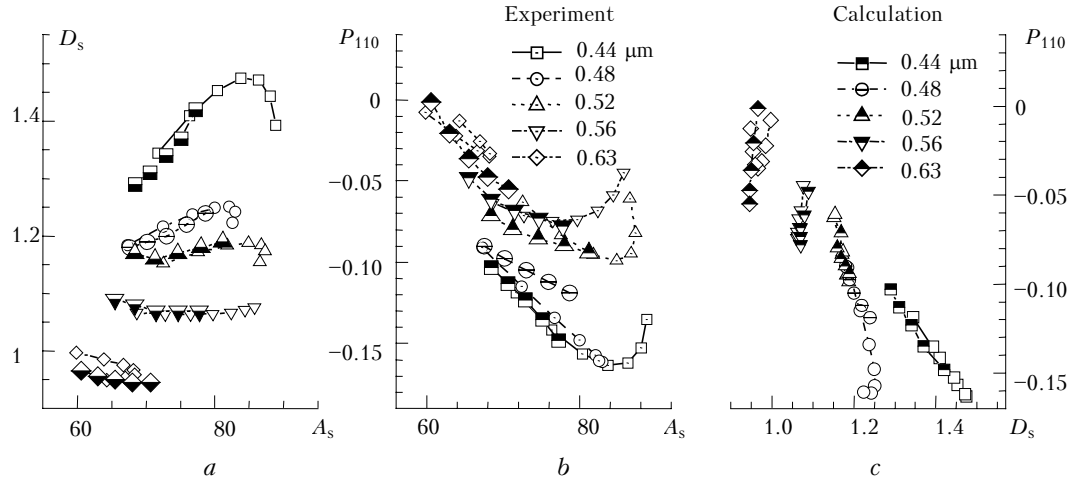

Fig. 2. Diagrams of mutual variations of the shape parameters of the scattering phase function D_s and A_s (*a*), the degree of polarization P_{110} and A_s (*b*), P_{110} and D_s (*c*) as judged from calculated data and laboratory measurements.

An example of optical diagrams of pyrolysis smokes that characterize the mutual dynamics of variations of these parameters at different wavelengths in comparison with the theoretically calculated data is shown in Fig. 2.

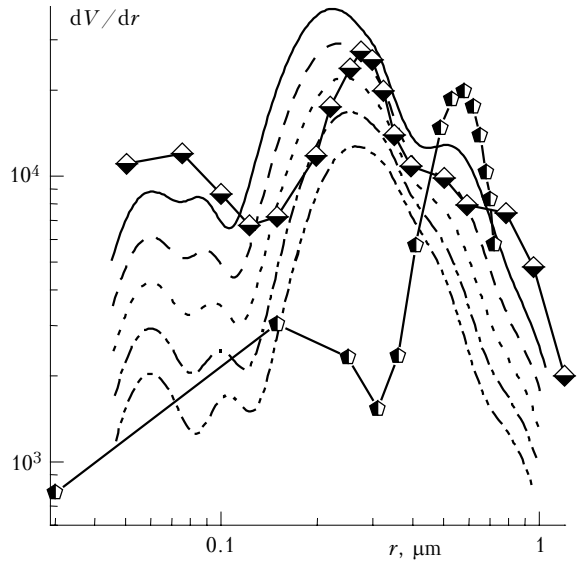

Fig. 3. Dynamics of the size spectrum of smoke aerosols, which provides for theoretically calculated parameters of the shape of the scattering phase function and degree of polarization shown in Fig. 2 in comparison with the data of Refs. 3 and 4 (symbols).

The results of direct simulation allowed us to outline the range of the most characteristic states of the smokes from the viewpoint of the microstructure, in particular, the characteristic range of variations of the particle size and the refractive index. Figure 3 illustrates the dynamics of the size spectrum of the smoke aerosols with the particle complex refractive index $m = 1.5 - i0.004$ corresponding to variation of the theoretically calculated shape parameters of the scattering phase function and the degree of polarization shown in Fig. 2. The similar data of Refs. 3 and 4 are shown in Fig. 3 for comparison (curves with symbols).

Comparison of the results of direct numerical simulation of the light scattering parameters with the measured data has shown that characteristic variations of the refractive index of the smokes generated at low-temperature pyrolysis decomposition of wood lie in a relatively narrow (in comparison with the estimates obtained in Refs. 3 and 4) range from 1.48 to 1.56. The volume distribution spectrum of smoke particles has a stable maximum in the range from 0.2 to 0.3 μm and undergoes complex irregular changes on the size scale. Optical manifestations of the particle fraction with the size ~ 0.45 to 0.65 μm are well seen at the initial stage of smoke formation. At later stages, the contribution of these particles decreases due to intense sedimentation of particles on the cell walls.

Then the estimated characteristic variation ranges of microstructure parameters obtained through direct simulation were used as additional *a priori* information when solving the inverse problem of light scattering.

To study the dynamics of the smoke microstructure parameters, we used the data characterizing simultaneous angular and spectral variations of the directional scattering coefficients $g(\theta_i, \lambda_j)$, where $i = 1, \ldots, 5$; $j = 1, \ldots, 9$. The regularizing algorithm was applied, in which the function $s(r) = \pi r^2 n(r)$ [μm/cm^3], where $n(r)$ is the density of size distribution of the particle number density, is determined based on its approximation by some stepwise function $s^*(r)$ (a histogram).[10] The function $s^*(r)$ is determined from minimization of the smoothing functional F_α in the k-dimensional vector space. The functional F_α, according to the Tikhonov's regularization method, can be written in the form

$$F_\alpha = \sum_i^5 \eta_i \sum_j^9 \Big(\sum_l^k q_{jl} S_l - q_j\Big)^2 +$$

$$+ \alpha \left[p_0 \sum_l^k S_l^2 + p_1 \sum_l^{k-1} (\Delta S_{l+1,l})^2 \right],$$

where p_0 and p_1 are the scale coefficients, α is the regularization parameter, $\{q_{j,l}\}$ are matrix elements calculated from the values of the scattering efficiency factor $K(r, \lambda)$ for a specific particle size and the corresponding scattering angle θ_i by quadrature formulas from Ref. 12, η_i are the weighting factors that regulate the relative significance of the used spectral dependences for different scattering angles. The components of the solution vector S_l form the total geometric cross section of particles in the ranges Δ_l with the boundaries r'_l and r''_{l+1}. The mean values of the stepwise function $s^*(r)$ in the above range are determined by the ratio S_l/Δ_l.

Different information capacity of the spectral dependences of the directional scattering coefficients measured at different angles with respect to the particle size spectrum and the refractive index allows us to formulate the problem of joint estimation of these parameters by the technique proposed in Ref. 13. For this purpose, discrepancies of spectral characteristics measured at different angles are combined into a single functional equation.

The inverse problem was solved and the peculiarities of variation of the smoke disperse structure for a specific realization were analyzed in several stages.

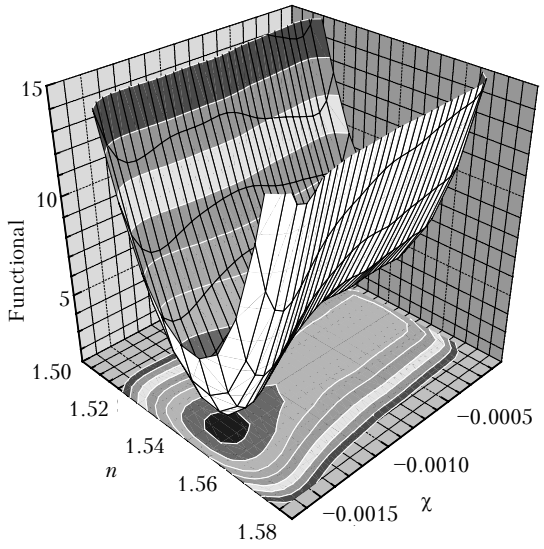

Fig. 4. Behavior of the smoothing functional F_α at the set of values of the real (n) and imaginary (χ) parts of the complex refractive index.

At the first stage, the boundaries of the size range, in which the distribution function $s(r)$ is positively defined, were revised for every realization of the laboratory experiment based on pre-solution of the inverse problem. Then the range of the most acceptable values of the real part of the refractive index n (Fig. 4) was estimated from the revised parameters of solution of the inverse problem based on the measured spectral dependences of the directional scattering coefficients at five angles through search of a minimum of the functional $F_\alpha[s(r), m]$, where $(m = n - i\chi)$. Analogously, the imaginary part of the refractive index χ was determined for already estimated n. At the final stage of solution of the inverse problem, the volume distribution of smoke particles dV/dr was reconstructed by use of the mean value of the refractive index from the determined range.

Results

As a first problem in the comprehensive investigation of the smoke aerosol, we considered the effect of the time, during which the smoke was let to stay in the chamber. Roughly the same temperature regime and duration (10 minutes) of pyrolysis were provided for this study. Wood samples (pine) of the same mass were taken. The burning temperature was measured with a thermocouple and controlled according to the value of the voltage applied to the heater by use of the voltage–temperature calibration characteristic. The time, during which the smoke was let to stay in the chamber, was taken to be t = 15, 30, 45, and 60 minutes. The reconstructed size spectra for these four cases are depicted in Fig. 5. They show the most significant variations in the smoke disperse composition in the size range up to 0.4 μm. These variations are largely caused by the coagulation growth of small particles due to their relatively higher number density, as well as more intense sedimentation onto the cell walls. A noteworthy fact is the presence of the second fraction $r \sim 0.6$ μm at the initial stages of smoke development at low-temperature decomposition of wood. The particle number density in this fraction decreases essentially at smoke aging. As a result, the right boundary of the size spectrum gradually shifts to 0.5 μm (Fig. 6).

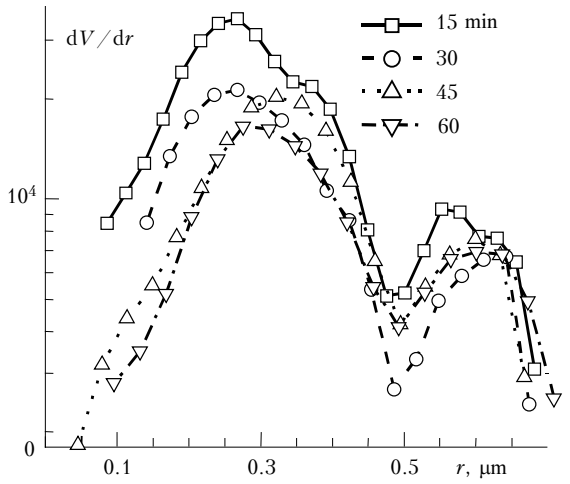

Fig. 5. Initial size spectrum of smoke aerosols depending on the time, during which the aerosol was let to stay in the chamber (T = 700°C).

The smoke microstructure parameters recorded once the aerosol was let to stay in the chamber for 15 minutes are presented in the Table. The table rows correspond to the measurement cycles (N is the number of cycle from the beginning of measurements). The parameters V_1, $\mu m^3 \cdot cm^{-3}$, S_1, $\mu m^2 \cdot cm^{-3}$, and R_{ef1},

μm, characterize, respectively, the particle volume, cross section, and mean radius up to the first minimum of the dS/dr distribution (Fig. 6*a*) $r \le 0.15$ μm. Analogously, the parameters V_2, S_2, and R_{ef2} correspond to particles having the size from the first minimum to the second one ($\sim 0.15 < r < 0.5$ μm). Estimates of V_3, S_3, and R_{ef3} are obtained for particles having the size larger than 0.5 μm. The index t at these parameters corresponds to the estimates obtained for the spectrum as a whole. The tabulated data show that the tendency to coagulation growth of particles can be seen in the behavior of the size spectrum of the second fraction up to the seventh measurement cycle. Then the number density significantly decreases, and the particle size spectrum changes largely due to intense particle sedimentation onto the cell walls.

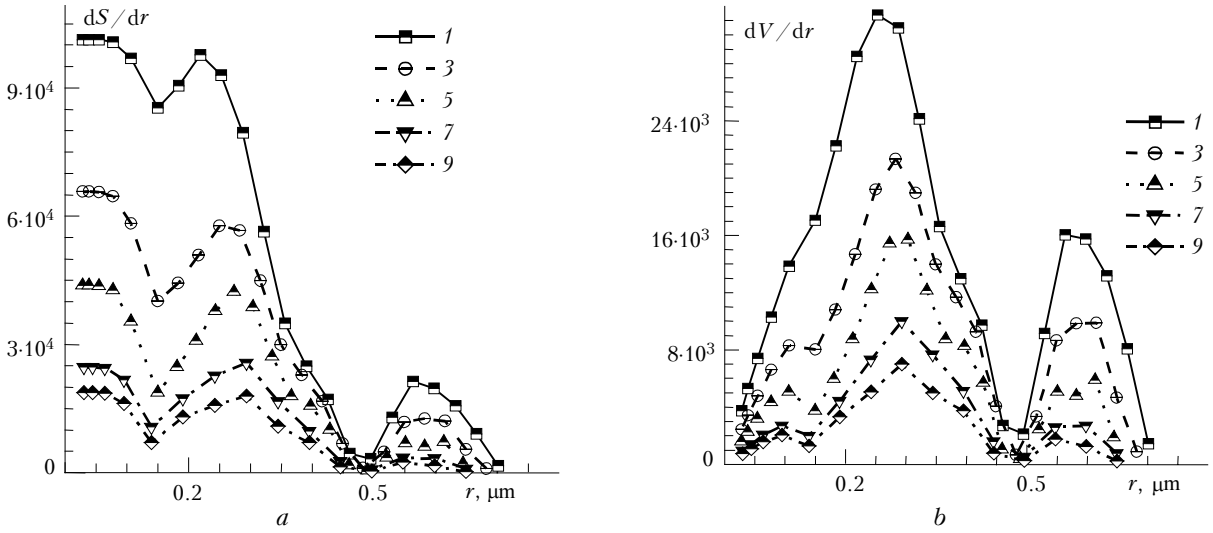

Fig. 6. Temporal behavior of the smoke particle size spectrum once the aerosol was let to stay in the chamber for 15 minutes (the curve number corresponds to the cycle number from the beginning of measurements, the total duration of measurements was ~ 80 min) (T = 700°C).

Cycle No.	$V_1 \cdot 10^{-3}$	$V_2 \cdot 10^{-3}$	$V_3 \cdot 10^{-3}$	$V_t \cdot 10^{-3}$	$S_1 \cdot 10^{-3}$	$S_2 \cdot 10^{-3}$	$S_3 \cdot 10^{-3}$	$S_t \cdot 10^{-3}$	R_{ef1}	R_{ef2}	R_{ef3}	$R_{ef\,t}$	R_2
1	1.68	6.03	2.19	10.11	13.72	17.48	2.77	33.77	0.092	0.258	0.594	0.225	0.735
3	0.63	4.42	1.26	6.33	6.58	12.83	1.62	20.73	0.073	0.259	0.586	0.229	0.715
5	0.40	3.04	0.63	4.08	4.25	8.32	0.83	13.40	0.072	0.274	0.574	0.229	0.653
7	0.29	1.84	0.34	2.47	2.68	4.84	0.44	7.97	0.081	0.286	0.573	0.233	0.640
9	0.20	1.50	–	1.71	2.22	4.09	–	6.32	0.069	0.276	–	0.203	0.505

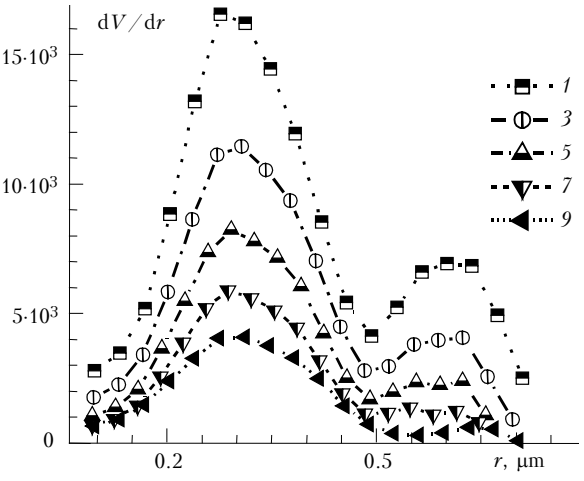

Fig. 7. Temporal behavior of the smoke particle size spectrum after the smoke was let to stay for 60 min (the curve number corresponds to the cycle number from the beginning of measurements, the total duration of measurements was ~ 80 min) (T = 700°C).

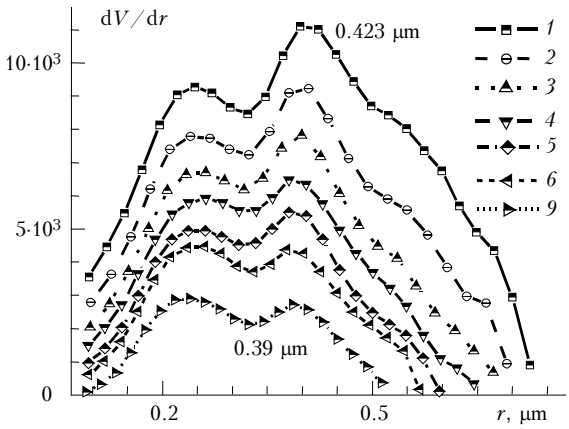

Fig. 8. Temporal behavior of the smoke particle size spectrum at low-temperature (490°C) pyrolysis (the curve number corresponds to the cycle number from the beginning of measurements, the total duration of measurements was ~ 80 min) (the smoke was let to stay for 10 min).

Once the solution is let to stay for 60 min, the size spectrum of small particles shifts to the right and the total number density of particles decreases (see Fig. 5). Therefore, only insignificant growth of small particles and essential sedimentation onto the cell walls are then observed (Fig. 7).

The variety of size spectrum shapes increases markedly as pyrolysis modes alternate. In particular, the relative content of large particles increases noticeably as the pyrolysis temperature decreases (Fig. 8). Particles having the size ~ 0.45 μm prevail over other fractions in the volume distribution, and some signs of large particles compacting are observed against the background of the sedimentation process. The distribution mode shifts to the range of small size by approximately 10% from the initial position. However, this result was revealed against the background of other factors, so it needs in more careful experimental examination.

Analysis of the results of spectral nephelometric measurements shows that the portion of particles having the size of 0.05–0.27 μm increases significantly with the increase of the pyrolysis temperature. The right boundary and the size spectrum of smoke particles determining the second distribution maximum noticeably shift toward the smaller size. If in Fig. 8 the right boundary of the size spectrum varies within 0.8–0.9 μm, then in Fig. 9, with the increase of the pyrolysis temperature, it even does not achieve 0.5 μm.

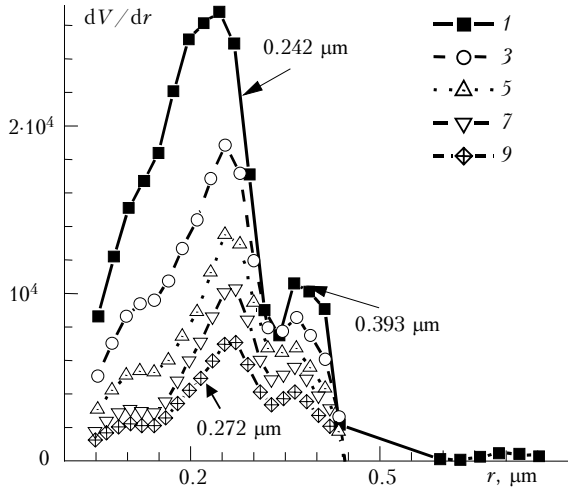

Fig. 9. Temporal behavior of the smoke particle size spectrum at low pyrolysis temperature (490°C) (the curve number corresponds to the cycle number from the beginning of measurements, the total duration of measurements was ~ 80 min) (the smoke was let to stay for 20 min).

The estimates of the imaginary part of the complex refractive index by the technique described above show that weak absorption is characteristic of smokes of pyrolysis origin, for which χ did not exceed 0.004 in all the considered cases.

The situation changes essentially when open flame arises. Figure 10 depicts the reconstructed size spectra of smoke particles generated at combustion. The estimates of the optical constants of the particulate matter show that the combustion smokes, in comparison with pyrolysis ones, absorb much more effectively and have the imaginary part of the refractive index $\chi \sim 0.050$. The real part of the refractive index also increases significantly: $n = 1.640$.

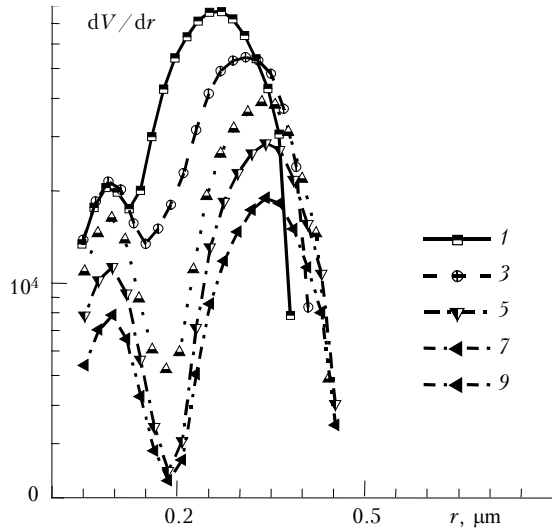

Fig. 10. Dynamics of the smoke particle size spectrum in the combustion mode (the curve number corresponds to the cycle number from the beginning of measurements, the total duration of measurements was ~ 80 min); combustion (flame) $m = 1.643 - 0.050i$.

These estimates are in good agreement with the conclusions of Ref. 7 about the influence of the wood burning mode on the soot content in smokes (these conclusions were drawn based on thermo-optical nephelometric investigations). A singularity in the dynamics of the size spectrum of particles having the size less than 0.17 μm is well pronounced. The tendency to particle coagulation growth is well seen in the size spectrum of particles with $r > 0.2$ μm, but the position of the mode of the fine fraction changes only slightly during development of the microstructure of combustion smokes. The decrease of the total content of particles belonging to this fraction is largely caused by particle sedimentation onto various surfaces. As the pyrolysis temperature increases essentially, the reconstructed spectra of all smokes have the rather sharp right boundary, whose position r_2 gradually increases from 0.33 to 0.45 μm in the case of combustion. On the contrary, the right boundary of smokes of high-temperature pyrolysis (without flame) shifts to the left from 0.48 to 0.39 μm.

The chamber was vented before every series of measurements, but it is rather difficult to exam the efficiency of this venting. So the possible influence of air conditions (in particular, air humidity at different stages of pyrolysis) inside the chamber on the size spectrum was also considered within this experiment. The results are shown in Figs. 11 and 12.

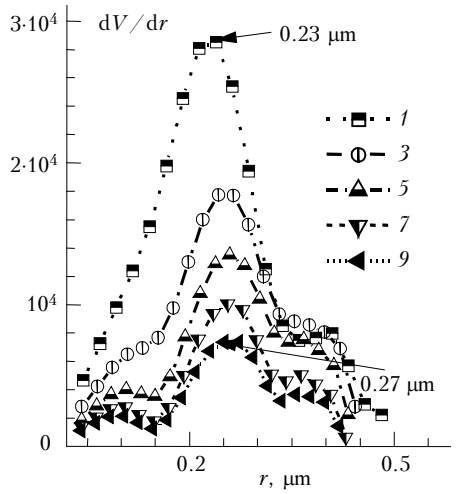

Fig. 11. Dynamics of the smoke particle size spectrum at pre-humidifying of the aerosol chamber (the curve number corresponds to the cycle number from the beginning of measurements, the total duration of measurements was ~ 80 min).

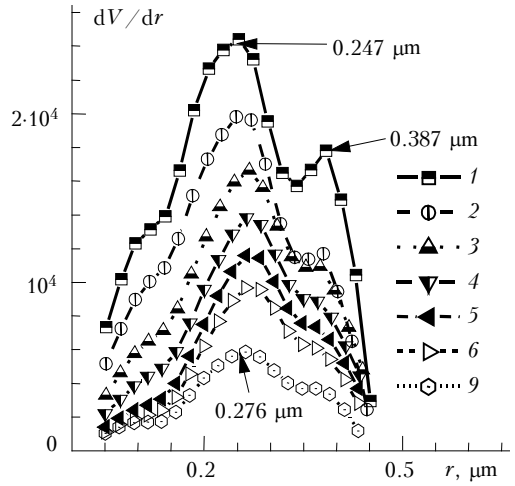

Fig. 12. Dynamics of the smoke particle size spectrum at humidifying the aerosol chamber just after pyrolysis (the curve number corresponds to the cycle number from the beginning of measurements, the total duration of measurements was ~ 80 min).

The analysis of the obtained data has shown that at chamber pre-humidifying (before pyrolysis) the position of the main maximum shifts to the left to $r \sim 0.21$ μm, and the concentration of these particles significantly increases. At the same time, the content of particles of the largest fraction does not undergo so noticeable dynamics. Humidifying of the chamber after pyrolysis causes more significant changes just in the composition of large particles, though the right boundary of the spectrum does not shift. No significant changes occur in the optical constants in this case.

Formation of optically active aerosol components (soot) in thermal decomposition of hydrocarbon fuels is usually related[14] to the processes determining formation of hydrocarbon radicals and skeletons of aromatic compounds (C_3, C_2H, C_2H_2, C_4H_2, C_6H_2, C_8H_2, etc.), which then take part in formation of hexagonal structures of carbon atoms arranged in one plane. A set of several such layers forms a soot crystal. A spherical soot particle 20–30 nm in diameter contains about 10^3–10^4 such crystals or ~ 10^6 carbon atoms.[14] As our estimates show, formation of actively absorbing particles is suppressed at low-temperature pyrolysis, and the imaginary part of the refractive index does not exceed 0.004. An attempt was undertaken to estimate the effect of ultraviolet irradiation on formation of the structure of pyrolysis smokes. Smoke aerosols were irradiated both at the stage of pyrolysis and at the subsequent stages of smoke microstructure development. Analysis of the obtained data has shown that the content of particles that determine the main maximum in the volume distribution noticeably increases (Fig. 13). As for combustion (see Fig. 10), the fine fraction of particles having the size ~ 0.05 to 0.09 μm was well pronounced at the subsequent stages of the smoke development. Active coagulation growth of the second mode of particles was not observed due to their lower number density, but the value of the complex refractive index changed somewhat. The search for a minimum of the Tikhonov functional has shown that the refractive index values optimal for solution of the inverse problem are 1.60 for the real part and 0.008 for the imaginary part. Perhaps all the peculiarities of this result follow from not only the specific influence of ultraviolet irradiation, but also from the increase of the temperature inside the chamber. This conclusion requires more detailed consideration in an experiment with controlled medium parameters.

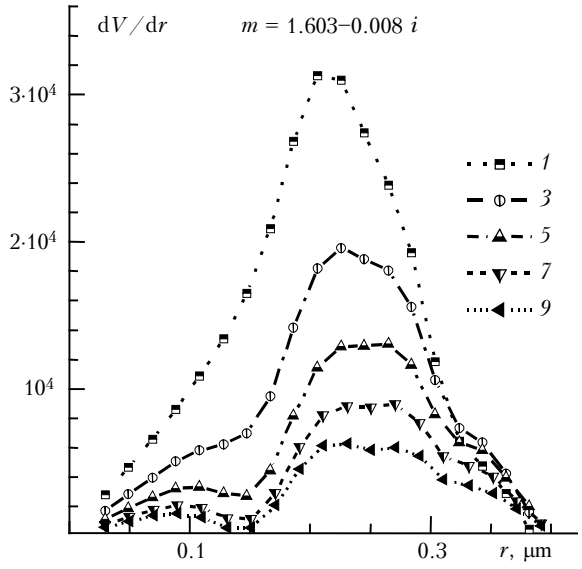

Fig. 13. Effect of ultraviolet irradiation on the dynamics of size spectrum of pyrolysis smokes (the curve number corresponds to the cycle number from the beginning of measurements, the total duration of measurements was ~ 80 min).

Conclusion

Summing up the results of analysis of the data of spectral nephelometric measurements, we can note the following peculiarities in the mechanism of low-temperature pyrolysis of wood materials:

– characteristic relatively narrow range of variations of the real part of the refractive index from 1.48 to 1.56, while the absolute values of the imaginary part do not exceed 0.004;

– several maxima in the size distribution of smokes (0.08, 0.25, and 0.45 μm) observed at different stages of smoke formation and development;

– the size spectrum shows the essential dependence on the pyrolysis temperature conditions and humidity in the chamber;

– the generation rate of particles with the size from 0.04 to 0.3 μm essentially increases with the increase of the temperature, the generated size spectrum as a whole shifts noticeably to smaller size, and this is especially true for its right boundary, whose values changes from 0.85 to 0.49 μm; some signs of compacting of large particles arise;

– at significant increase of temperature and appearance of flame (combustion), in addition to the mentioned changes in the disperse structure, the real and imaginary parts of the refractive index change considerably, and the absorption efficiency increases almost 50 times.

Acknowledgments

This work was supported in part by the Russian Foundation for Basic Research (Grant No. 00–03–32422a).

References

1. V.V. Veretennikov and V.S. Kozlov, in: *Investigation of Atmospheric Aerosol by Laser Sensing Methods* (Nauka, Novosibirsk, 1979), pp. 186–201.
2. V.V. Veretennikov, V.S. Kozlov, I.E. Naats, and V.Ya. Fadeev, Izv. Akad. Nauk SSSR, Ser. Fiz. Atmos. Okeana **16**, No. 3, 270–276 (1980).
3. A.A. Isakov, Atmos. Oceanic Opt. **12**, No. 1, 20–27 (1999).
4. A.A. Isakov, V.V. Lukshin, and M.A. Sviridenkov, Izv. Akad. Nauk SSSR, Ser. Fiz. Atmos. Okeana **24**, No. 3, 258–261 (1988).
5. R.F. Rakhimov, V.S. Kozlov, M.V. Panchenko, A.G. Tumakov, and V.P. Shmargunov, Atmos. Oceanic Opt. **14**, No. 8, 624–628 (2001).
6. R.F. Rakhimov and V.S. Kozlov, Atmos. Oceanic Opt. **11**, No. 9, 792–798 (1998).
7. V.S. Kozlov and M.V. Panchenko, Fizika Goreniya i Vzryva **32**, No. 5, 122–133 (1996).
8. V.V. Lukshin and A.A. Isakov, Izv. Akad. Nauk SSSR, Ser. Fiz. Atmos. Okeana **24**, No. 3, 250–257 (1988).
9. V.N. Sidorov, Izv. Akad. Nauk SSSR, Ser. Fiz. Atmos. Okeana **24**, No. 3, 262–273 (1988).
10. B.S. Kostin, E.V. Makienko, and I.E. Naats, in: *Problems of Remote Sensing of the Atmosphere* (Tomsk Affiliate of Siberian Branch of the Academy of Sciences of the USSR, Tomsk, 1976), pp. 86–97.
11. A.N. Tikhonov and V.Ya. Arsenin, *Methods for Solution of Ill-Posed Problems* (Nauka, Moscow, 1974), 224 pp.
12. I.E. Naats, *Theory of Multifrequency Laser Sensing of the Atmosphere* (Nauka, Novosibirsk, 1980) 157 pp.
13. E.V. Makienko and I.E. Naats, in: *Problems of Remote Sensing of the Atmosphere* (Tomsk Affiliate of Siberian Branch of the Academy of Sciences of the USSR, Tomsk, 1976), pp. 42–56.
14. F.G. Bakirov, V.M. Zakharov, I.Z. Polyshchuk, and Z.G. Shaikhutdinov, *Formation and Burn-out of Soot at Burning of Hydrocarbon Fuels* (Mashinostroenie, Moscow, 1989), 128 pp.